Human Emissions Drive Recent Trends in North Pacific Climate Variations

Jeremy M. Klavans[1*], Pedro N. DiNezio[1], Amy C. Clement[2], Clara Deser[3], Timothy M. Shanahan[4], Mark A. Cane[5]

[1]Department of Atmospheric and Oceanic Sciences, University of Colorado Boulder; Boulder, CO, USA.

[2]Rosenstiel School of Marine, Atmospheric, and Earth Science, University of Miami; Miami, FL, USA.

[3]National Center for Atmospheric Research; Boulder, CO, USA.

[4]Jackson School of Geosciences, University of Texas at Austin; Austin, TX, USA.

[5]Lamont Doherty Earth Observatory, Columbia University; New York, NY, USA.

*Corresponding author. Email: jeremy.klavans@colorado.edu

Abstract

The Pacific Decadal Oscillation – the leading pattern of climate variability driving changes over the North Pacific and surrounding continents – is currently thought to be generated by processes internal to the climate system. These internal variations in climate ought to have altered the phase of the PDO. However, this mode has been locked in a consistent downward trend for more than three decades, remanding nearby regions to a steady set of climate impacts. Using an exceptionally large ensemble of climate model simulations, we show that major multidecadal variations in the PDO index during the 20th century, including the current decades-long negative trend, were largely driven by human emissions of aerosols and greenhouse gases rather than internal processes. This anthropogenic influence was previously undetected because the current generation of climate models systematically underestimate the amplitude of forced climate variability. A novel attribution technique that statistically corrects for this error suggests that observed PDO impacts – including the ongoing multidecadal drought in the western United States – can be largely attributed to human activity via externally forced changes in the PDO. These results suggest that we rethink the attribution and projection of multidecadal changes in regional climate.

The Pacific Decadal Oscillation (PDO) – the leading mode of North Pacific sea-surface temperature (SST) variability[1, 2] – is not oscillating. The ongoing, stubbornly persistent, cold phase of the PDO is associated with significant long-term trends in climate, including the rate of global warming[3] and drought in the western United States (U.S.)[4]. The leading conceptual models suggest that the PDO varies in response to an accumulation of processes internal to the climate system, including random atmospheric circulation variability, local ocean dynamics, and coupled tropical variability[5-7]. Statistical and dynamical models that simulate these processes predicted that the massive 2015 El Niño would finally reverse the sign of the obstinately persistent PDO[8]. Yet, the PDO and its associated impacts remain unchanged.

An alternative explanation for the PDO is that it reflects a North Pacific ocean-atmosphere response to external radiative forcings. However, the conventional understanding of the PDO does not include external radiative forcing; recent review studies and the latest comprehensive report from the Intergovernmental Panel on Climate Change express "high confidence" that multidecadal North Pacific climate variability is internally generated[5, 7, 9, 10]. New research shows that large changes in the emissions of aerosols and greenhouse gases may explain recent multidecadal variations in North Atlantic and European climate[12–15], although this view is somewhat controversial[16]. A developing line of research hints that similar processes may be at play in the North Pacific[17–24] but this work cannot fully explain the persistence of the ongoing negative phase of the PDO or why models underestimate levels of PDO variance[7,25,26] .

Here we isolate anthropogenic influences on multidecadal North Pacific climate variability using an exceptionally large ensemble of climate model simulations. We characterize climate variability in the North Pacific using the first principal component of North Pacific annual average SST anomalies as a PDO index[2]. We calculate these anomalies by removing the annual cycle and subtracting global mean temperature[2]. This definition, which avoids the constraint that the PDO must be orthogonal to global temperature rise[2], is widely used in recent mechanistic and impact studies of the PDO[4,5] and we wish to bring PDO impacts to the forefront. We calculate the PDO index in each of the 572 simulations in the multi-model ensemble, all of which are forced by a combination of all the major sources of external forcing, including greenhouse gas and aerosol emissions, volcanic eruptions, and solar variability (Table S1). Averaging the historical PDO indices simulated by all ensemble members cancels out uncorrelated, naturally generated variations in climate, revealing the externally forced influence common to all simulations. We further isolate individual sources of external forcing by considering three "single-forcing" large ensembles, each of which includes changes in only one forcing agent at a time (Table S2). The bulk of our analysis focuses on the 1950-2014 period common to all simulations, although we consider the full length of simulations dating back to 1850 when possible. On interannual timescales, the PDO index is in-part driven by the El Niño – Southern Oscillation (ENSO), a prominent source of naturally-generated variability[5, 27]. As noted above, ensemble averaging removes the influence of the internal component of ENSO on the

PDO index in models [2, 28, 29]. We linearly remove variability associated with the Nino 3.4 index from the observed PDO index to isolate the sources of multidecadal variability that are the focus of this manuscript (Methods). While this approach slightly alters the interannual timing of the observed PDO index, it has limited effect on the multidecadal shifts in the index that we are seeking to explain (Fig. S1). Therefore, removing the effect of ENSO on the PDO allows us to better analyze the less-well-known drivers of multidecadal variability and their signal-to-noise characteristics. Finally, we low-pass filter both the observed and simulated PDO indices to isolate variability with periods longer than 10 years (Methods).

We find that changes in external forcing explain key recent multidecadal shifts in observed North Pacific climate. Between 1950 and 2014, we estimate that the externally forced PDO index explains 53% of observed multidecadal PDO index variance (R^2) and reproduces major PDO transitions in the 1970s and 1990s to within a few years, even without accounting for tropical Pacific variability (Fig. 1a). External forcing explains 46% of PDO index variance in a stricter, alternative definition of the PDO index, wherein North Pacific regional temperatures are subtracted (rather than global mean temperatures) to ensure that our conclusions are not an artifact of a known relationship between Pacific climate variability and global mean temperatures (Fig. S2a)[30]. Likewise, external forcing explains 48% of the detrended, decadal SST variance in the crucial Kuroshio-Oyashio Extension (KOE) region, demonstrating that our results are not an artifact of the traditional approach to isolating PDO variability with Empirical Orthogonal Functions (Fig. S3a). The reported levels of variance explained for the traditional PDO index, the PDO index with North Pacific SSTs removed, and the KOE SST index are statistically significantly different from zero at the 4%, 6%, and 4% levels via a non-parametric statistical test that accounts for serial correlation in low-pass filtered timeseries[31] (Methods; Table S3).

The statistical tests above do not account for the possibility that internal variability in observations happens to align with the ensemble mean, thereby amplifying the reported correlation coefficients by chance. We find this possibility to be unlikely. The model-estimated, forced PDO index explains more variance in the observed PDO index than more than 99% of the model-generated realizations of internal variability (568 out of 572; Fig. 2a). That is, in models, there is less than a 1% chance (4 out 572 realizations) that internal variability alone explains the correlation between the ensemble mean and observations (Fig. 2a). Likewise, the model-estimated, forced PDO index explains more variance in the observed PDO index than in 98% of the individual model simulations (560 out of 572; Fig. 2b). That is, in models, there is a 2% chance (12 out of 572 realizations) that internal variability aligns with external forcing to increase the apparent share of forced variance in the PDO (Fig. 2b). Conversely, external forcing can consistently explain the large correlation we report above (Fig. 2c).

Our approach was able to isolate this unexpectedly large influence of external forcing on the PDO because of the extremely large number of model simulations that have recently become available. We estimate that more than 70 individual ensemble members are required to isolate the forced component of the PDO; that is, 70 members are needed to reach a correlation with observations that is not significantly different (at the 95% level) from the estimate from the full

ensemble (Fig. 2d; Fig S4). These extraordinarily large datasets are needed because models underestimate the amplitude of the forced component of the PDO. In observations, external forcing accounts for 53% of total multidecadal PDO amplitude whereas in models, external forcing only accounts for 7% of total multidecadal PDO amplitude (Methods). This error is also apparent in the KOE SST index, for which external forcing accounts for 48% of observed multidecadal variance and 7% of simulated multidecadal variance. Put succinctly, in models, the ratio of the externally forced signal to internally generated "noise" in the multidecadal PDO is much lower than in observations. Consequently, the much too large internally generated noise overwhelms the forced PDO and KOE SST signals in the individual simulations of historical climate. This signal-to-noise error is also apparent in simulations of North Atlantic climate variability, indicating that this error may affect low-frequency climate modes of variability throughout the extratropical Northern Hemisphere, and potentially globally[13, 32 – 35].

The contribution of external forcing to the PDO grows as external forcing intensifies throughout the 20th century. Prior to the mid-20th century, PDO variability in models appears to be largely internally generated by the climate system (Fig. 2e)[17]. Between 1870 and 1950, external forcing explains less than 1% of multidecadal PDO variance (Fig. 2e). However, after the mid-20th century, as changes in forcing dramatically increase, so too does the role of external forcing in the PDO (Fig. 2b; Fig. S5). Likewise, the variance of the forced component increases after the mid-20th century for both the PDO index and the KOE SST index (Table S4). The variance of internal KOE temperature variability in models does not change between 1870 - 2014, like in the North Atlantic[36], suggesting that signal and noise may be additive in climate models (Table S5). Prior studies may have underestimated this newfound role of forcing in the PDO for two reasons: they could only utilize small ensembles and they may have convolved the relatively unforced first half of the 20th century with the intensifying forcing of the second half of the 20th century. For example, in an average 40-member ensemble run from 1920 – 2005 (as in [5]), external forcing explains only 5% of multidecadal PDO variance. To detect the role of forcing in the modern PDO, one must use an exceptionally large ensemble and focus on the late 20th century (i.e. after 1950), when changes in forcing were larger.

The size and breadth of this ensemble allow us to demonstrate the robustness of this new, larger role for external forcing in the PDO. First, we find that both single-model ensembles (CESM2 and MPI) that meet the criterion of 70 members to sufficiently isolate the forced PDO (Fig. 2d) have a statistically significant forced component (Fig. S5). While it is likely that there are inter-model differences in the amplitude of the forced response, the signal-to-noise error makes it difficult to make definitive statements about single-model ensembles with less than 70 members. Instead, we group models by their common attributes and create large enough ensembles to isolate the impact of these features on the forced PDO. We find that the contribution of forcing to the PDO is reasonably robust to (1) model generation, i.e. CMIP5 or CMIP6, (2) the implementation of aerosol emissions, and (3) the complexity of cloud-aerosol interactions (Fig. 2f; Table S6). That is, both the anthropogenic influence on the PDO and the signal-to-noise error in the forced response is robust across models despite their diverse representations of physical processes (Table S6). Together these sensitivity analyses show that

the substantial role for external forcing in the timing of the PDO index is not an artifact of a single model, numerical approach, or physical process, such as the implementation of aerosol indirect effects.

Models show that the observed timing of multidecadal shifts in the PDO index are influenced by a combination of anthropogenic aerosols and greenhouse gasses. Between 1950 and the mid-1980s, rapidly rising concentrations of industrial aerosols[37,38] coincide with a positive trend in the PDO index (Fig. 1a; Table S6). When forced with only industrial aerosols, models also simulate a positive PDO trend over that period (Fig. 3a and 3d; Table S7). In the late-1980s, the observed positive PDO trend reverses in association with stagnating aerosol emissions[38] and the predominance of greenhouse gas warming (Fig 1a, 3a, and 3b; Table S7)[7]. The observed negative trend in the PDO after the mid-1980s is captured in the all-forcing runs and is even stronger when models are forced with only greenhouse gases, which drive a negative trend in the PDO (Fig. 3b and 3d; Table S7). We note that the short length of this subsection of the record limits its statistical significance (Tables S6 and S7); however, these trends have continued and intensified to present day consistent with our argument. We suggest that stagnating industrial aerosol concentrations paired with rising greenhouse gas concentrations halted the rise in the PDO index in the mid-1980s and produce the negative trend in the PDO index that continues into the present. Both anthropogenic aerosols and greenhouse gases can force changes in the PDO, whereas small changes in natural forcings, i.e., from solar cycles and volcanic eruptions, only explain a small part of the temporal evolution of the PDO over our study period (R^2=1%, Fig. 3c and 3d).

In addition to explaining key observed shifts in the PDO, the forced PDO index is associated with an SST pattern in models that bears key resemblances to both the observed PDO pattern and the internally generated PDO pattern in models. In the PDO positive phase, the observed and simulated SST patterns both show cooler than normal ocean temperatures over the western and central North Pacific, surrounded by a horseshoe of relatively warmer surface waters along the North American coast (Fig. 1b and 1c; Fig. S6). Like the real world, the positive phase of the forced PDO in models is associated with a deepening of pressure near the Aleutian Low, the semi-permanent low-pressure system controlling surface winds over the North Pacific (Fig. 1c, contours). If the PDO index was purely internally generated, this pattern would not appear in the regression on the ensemble mean as it would cancel out across many ensemble members. The general features of the forced PDO pattern are robust across model generations, individual model ensembles, and how models represent complex physical processes (Fig. S6, S7, and S8). Yet, the multi-model mean and most individual ensembles exhibit one key deficiency: the horseshoe-shaped pattern of warming along the coast of North America in the positive phase of the PDO appears to be weaker in models than observations (Fig. 1b, Fig. 1c, Fig. S6, Fig. S7, and S8). This deficiency appears to be related to models' ability to generate the full PDO pattern, not just its externally forced component (Fig. S6).

The discrepancy between the spatial patterns in observations and the ensemble mean may offer a clue as to why the forced PDO is too weak in models. The horseshoe-shaped pattern of

temperature anomalies is characteristic of the well-established simultaneous relationship between the Aleutian Low and North Pacific SSTs in observations[5]. In models, we find that the forced, multidecadal PDO index is highly correlated with forced variations in the strength of the forced, multidecadal Aleutian Low (R^2=0.7; Fig. S9b; Methods). This indicates that either variations in the Aleutian Low drive changes in the PDO SST pattern[5] or SST variations, particularly in the KOE region, can drive changes in the overlying Aleutian Low[39-41]. Either of these potential responses could be excited by hemispheric warming or cooling, including contemporaneous forced North Atlantic climate variability[42] or over nearby continents[43,44].

Any of these pathways would rely on an amplifying feedback over the KOE region whereby oceanic thermal advection by wind-driven ocean currents reinforces SST variability[45]. We find that the strength of the relationship between the Aleutian Low and SSTs is much weaker in models (average ensemble member 1.5 hPa/degC, forced component 0.9 hPa/degC; Fig. S9c) than in observations (5 hPa/degC; Fig. S9d), which we quantify by regressing sea-level pressure variations on SST variations in the KOE region. This suggests that in models, perturbations fail to excite a response in the Aleutian Low with the same vigor as the real world. This mismatch might occur either due to poor simulation of the direct influence of forcing on the atmosphere or an underestimated positive feedback involving KOE SSTs[46]. In either case, these underestimated mechanisms, could help explain the underestimated amplitude and persistence of the forced PDO in models.

The failure of climate models to simulate the full amplitude of the forced PDO has clouded our view of the recent history of global and regional climate. In the early 2000s, a "hiatus" in global warming was largely attributed to a naturally generated PDO-like pattern of cooling in the Pacific Ocean[3, 47]. However, we have shown that forcing excites this pattern on multidecadal timescales, but its influence is underestimated by climate models. Mitigating the signal-to-noise error in climate models will amplify the forced PDO so they will better account for global mean temperatures at the beginning of the 21st century. Further, by mitigating this error in models we may also rectify known biases in the simulation of externally forced trend in the tropical Pacific [48]. Although here we demonstrate that forcing excites the PDO pattern in isolation from the tropics, climate variability in these two regions is intertwined[5]. Overall, climate models incorrectly simulate a forced El Niño-like trend in the tropical Pacific over the last few decades[49], which is at odds with the neutral or La Niña-like trend in observations and theory[48, 50, 51]. This erroneous trend appears uniquely within the tropics[28]. We show that the ongoing negative trend in the extratropical PDO, including the associated cooling that extends into the eastern tropical Pacific, is underestimated by models. If the signal-to-noise error were to be corrected in models, it follows that the cooling simulated by models in the eastern tropical Pacific could be enhanced through the extratropical influence of the forced PDO to be brought into better agreement with observations.

The meteorological drought in the western US is currently thought to be internally generated by a natural, albeit unlucky, combination of variations in the climate system. This idea prevails because climate models do not explain the magnitude of the observed precipitation

decline.[52, 53] However, it is established that the PDO is associated with precipitation in the western U.S.[8, 54] Thus our findings that models underestimate the forced response of the PDO suggest that the meteorological drought has a large anthropogenic component. We correct for this error by setting the signal-to-noise ratio in models equal to our estimate of that in observations[35] (Methods). We retain random interannual variability in each ensemble member but reduce its amplitude and increase the amplitude of the forced PDO and associated impacts (Fig. 4a and 4b). After this correction for the signal-to-noise error, we find a much larger precipitation deficit in the western U.S. than the original ensemble (-12.6% compared to -2.1% of climatology per 30 years), bringing them close to observations (-13.3%; Figs. 4c, 4d, and 4e)., Negative precipitation trends as large as observed are commonplace in the statistically corrected ensemble but were rare in the original ensemble (47% of simulations compared to 12%). Correcting for the signal-to-noise error in climate models attributes nearly all of the observed long-term precipitation decline over the last few decades to anthropogenic forcing, via the forced PDO. In addition to the forced PDO, there is also a role for internally generated tropical Pacific sea-surface temperature variability in setting western U.S. precipitation rates[52,55]. A complete analysis of the role of forcing in the meteorological drought would have to account for uncertainty in the magnitude of the signal-to-noise error in PDO impacts, how the signal-to-noise error changes in response to different combinations of forcing agents, and possibility that observed internal variability confounds our estimate of the observed, forced signal. We find the last of these sources of uncertainty unlikely to influence our results (Methods).

While our results emphasize the newfound role for external forcing in the PDO and its impacts, internal variability is an important contributor, especially on interannual and shorter timescales. For example, internal variations in ENSO influence the PDO on interannual timescales[5, 8] and therefore accurate ENSO predictions can add skill to near-term PDO predictions[56, 57]. Model errors in the tropical Pacific or elsewhere may deleteriously influence our results on the PDO and its impacts, as in any study reliant on models. Because our estimate of the magnitude of the forced PDO is based on correlations, underestimating the internal component of the PDO[25] is one error that does not affect our results (Methods). A subset of models with a realistic internally generated PDO produce a forced PDO that is well-correlated with observations but nonetheless exhibit the signal-to-noise error, as in the full ensemble (Fig. S11). Thus, our estimates of the role of external forcing in the PDO stand up to knowable forms of uncertainty but are still bound by the limitations of any modeling study.

Overall, we find that human activity is a key contributor to multi-decadal trends in the PDO since the 1950s. Aerosol emissions influenced the positive trend in the PDO from the 1950s to 1980s. The abatement of industrial aerosol emissions paired with exponentially rising greenhouse gas emissions are influencing the ongoing negative trend in the PDO. This history of external forcing can thus explain a significant portion of multidecadal PDO impacts over the past seven decades, including the ongoing drought in the western U.S. as shown here. The role of external forcings in the PDO was obscured by an unrealistically low signal-to-noise ratio in climate models, which we can expose only because we now have an extraordinarily large ensemble of climate model simulations. We suggest that the small amplitude of the forced PDO

is related to an underestimated Aleutian Low response to external forcing in models. By identifying this error in the North Pacific, we have added to results for the North Atlantic[13], showing that the signal-to-noise error is a pervasive problem across the extratropics in the Northern Hemisphere. Resolving the signal-to-noise error therefore offers the prospect of improvements in predictive skill for regional climate in climate models based on projections of external forcing. At the very least, it would allow equivalent skill with far smaller ensembles.

Model improvements, such as increasing spatial resolution, may help mitigate the signal-to-noise error[57, 58] by improving the simulation of both oceanic[59, 60] and atmosphere-ocean feedbacks[46, 61]. Of course, model development is expensive and time consuming. While we await improvements in models, reinterpretation of the existing catalogue of climate model output holds the potential to improve our understanding and ability to project regional climate changes. For example, because of the signal-to-noise error in climate models, the prevailing view has been that the ongoing historical western U.S. meteorological drought is a natural variation associated with the oscillating internal PDO. Thus, it is expected to abate when the PDO reverses sign. In our reinterpretation of model output, we project that so long as ongoing anthropogenic forcing trends continue, the PDO will remain persistent in its negative state driving continued precipitation deficits in the western U.S. The difference is obviously highly consequential.

Methods

Models

We study an extremely large collection of climate model simulations from the last two generations of model development (Table S1). This collection is composed of simulations from 13 individual climate models. We choose models that have at least 20 publicly available simulations each. All simulations are forced with the best estimates of observed external forcing for the full length of each run. The climate trajectory in each simulation is composed of a unique sequence of internally generated variability not necessarily correlated with the observed variability plus an externally forced response common to all simulations. The forced response includes both anthropogenic global warming and regional climate changes and is isolated by averaging changes in a given climate variable, such as SST, across many simulations[62]. We consider the time period common to all members, 1950 - 2014. Note that for CMIP5 models, 2006 – 2014 is forced with scenario forcing, not observations. We also consider single-forcing runs from DAMIP[63]. As mentioned in the main text, each of these runs are forced with one time-varying source of external forcing (industrial aerosols, greenhouse gases, or natural sources) while the others remain constant.

Observations

We compare the simulations used in this study to the PDO index as calculated by the National Oceanic and Atmospheric Administration (NOAA) National Centers for Environmental Information, using NOAA's Extended Reconstructed Sea Surface Temperature version 5[64]. To check for robustness, recalculate the PDO index from the gridded Hadley Centre Sea Ice and Sea Surface Temperature (HadISST) dataset[65]. This sea surface temperature (SST) dataset is also used for the observed temperature maps presented herein. To consider the pattern and strength of the atmospheric circulation over the North Pacific, we use NCEP/NCAR twentieth Century Reanalysis v2c[66]. For estimates of Southwestern U.S. precipitation, we use a 1° × 1°

configuration of the Global Precipitation Climatology Project version 2018 (GPCP) gridded monthly precipitation product covering the years 1901–2014[67].

Indices

In each individual simulation, first calculate monthly SST anomalies relative to the climatological seasonal cycle. We next calculate the PDO index as the first EOF of North Pacific (20° – 80°N) monthly SST anomalies, after subtracting the global mean SST anomaly from each month at each grid point (*2*). We choose this index because of its historical and ongoing value in forecasting climate impacts[1, 68]. Further, by removing global mean SST we show that the relationship between forcing and the PDO is more than the obvious GHG-induced warming trend. (An alternative definition of the PDO index that removes North Pacific average SSTs instead of global average SST yields qualitatively similar results for the metrics we put forward in the main text; Fig. S1). To calculate the forced component of the PDO index in models, we average each of these individual PDO indices together. We follow the convention that the PDO is positive when there is warming along the coast of North America paired with cooling off the coast of Japan[5]. The Kuroshio-Oyashio Extension index is calculated as the linearly detrended, area-weighted average SST between 25° – 35°N and 150° – 180°E[7]. The North Pacific Index, a measure of Aleutian Low strength is calculated as the area-weighted average sea-level pressure between 35° - 65°N and 160°E – 140°W[61]. The western US precipitation index is the water-year average (Oct. – Sep.), area-weighted average total precipitation between 31° – 42°N and 125° – 110°W, over land (following [46]). The El Nino-Southern Oscillation (ENSO) is summarized via the Nino 3.4 index, the area-weighted average monthly SST anomalies in the tropical Pacific (5°S-5°N, 170°W – 120°W). The forced component any of these indices is calculated as the average across all simulations of the individual indices. The externally forced temperature, pressure, and precipitation maps are calculated by first finding the ensemble mean field and then calculating any appropriate regression. In this construction of the ensemble mean, each ensemble member, not each model, is weighted equally. All timeseries are low-pass filtered using a 100-point Lanczos filter with a 1/10 year half-power frequency, unless otherwise noted. Endpoints are padded with the mean of the timeseries. Other approaches, including padding with zeros, repeating endpoints, and removing endpoints, were all tested and did not impact our results. For the observed PDO index we remove the ENSO signal via linear regression. It is likely that this simple method does not fully remove the influence of ENSO on the PDO (e.g. [27]).

Statistical significance

Throughout the manuscript we test several complementary null hypotheses to ensure robustness and transparency in our results. To probe the null hypotheses that our test statistic, the Pearson correlation coefficient, is statistically distinct from zero, we employ a commonly used empirical statistical test[31]. This test creates surrogate ensemble mean PDO timeseries by re-shuffling the phases of its periodogram. Each surrogate timeseries therefore has the same autocorrelation structure as the original timeseries. We correlate the surrogate timeseries with the observed timeseries and repeat the process 10,000 times to create a distribution. We compare the original correlation to this distribution.

We recognize that any purely statistical test of significance is limited by the very few realizations of the multidecadal trends. Therefore, we take advantage of the power of the large ensembles to test additional null hypotheses. For example, to test the null hypothesis that the correlation between the ensemble mean and observations is a chance result of internal variability, we remove the ensemble mean PDO from the PDO index in each individual member to estimate

the internal-only PDO (Fig. 2a). Similarly, we test the possibility that the combination of forcing and internal variability contrives to produce the forced correlation by creating a distribution of correlation coefficients between the total PDO index in each ensemble member and observations. Additionally, to test the null hypothesis that the ensemble mean is isolating forced variability, we randomly resample individual model runs (with replacement) 10,000 times to construct new ensembles of varying sizes (Fig. 2d). We find that the average ensemble mean PDO index from a 572-member ensemble produces a correlation of 0.71 (95% confidence interval: 0.66 – 0.76) with observations. Likewise, we find that the average ensemble mean KOE SST index from a 572-member ensemble produces a correlation of 0.57 (95% confidence interval: 0.51 – 0.62) with observations. The mean values are slightly different from the full ensemble values presented in-text because we re-sample with replacement. Over the course of this manuscript, each assertation is typically subject to several of these tests, as appropriate.

Estimating the signal-to-total variance ratios in models and observations and a novel attribution technique that accounts for the signal-to-noise error in climate models

We are interested in isolating the role of forcing in observations but are only privy to only one realization of Earth's climate. The (unknowable) *true* forced response $O_F(t)$, is a component of the observed timeseries: $O(t)$:

$$O(t) = O_F(t) + O_I(t)$$

where, $O_I(t)$, is the (unknowable) internally generated variability in the observed time series. We estimate the forced response by a regression on the ensemble mean $EM(t)$ of model runs

$$O_F(t) = \beta\, EM(t) + \epsilon$$

The fraction of observed variance explained by this regression model is:

$$R_i^2 \equiv \frac{\sigma_F^2}{\sigma_O^2} \approx \frac{\sigma_{EM}^2}{\sigma_O^2}$$

where, σ_F^2, is the (unknowable) forced variance, σ_O^2 is the total observed variance and σ_{EM}^2 is the variance of the model ensemble mean.

Unlike observations, in large ensembles we know the ratio of forced-to-total variability, R_j^2. We estimate it as the variance of the ensemble mean, σ_{EM}^2, divided by the average of the total variance in each ensemble member, σ_E^2:

$$R_j^2 = \frac{\sigma_{EM}^2}{\sigma_E^2}$$

There are other ways to estimate this fraction of model variance that is forced; e.g. we could find R_j as the average correlation of each of the ensemble members with the ensemble mean. As ensemble size j increases the various estimates converge asymptotically and with our sample size of 572 the differences are negligible ($R < 0.01$). As we discuss in-text and show in Table S6, our estimate of the observed forced variance ratio, R_i^2, is much larger than the ratio that we estimate

from our large ensemble, R_j^2. It follows that the (estimated) observed signal-to-noise ratio, $R_i^2/(1-R_i^2)$ is even larger compared to the model signal-to-noise ratio, $R_j^2/(1-R_j^2)$. The mismatch between these two ratios is known as the "signal-to-noise paradox"[29-32].

To estimate the impacts of the forced PDO we statistically correct for this signal-to-noise error in models. We do so by rescaling the variance of the multidecadal, forced PDO and its impacts in each simulation so that the signal-to-total ratio of the PDO index is the same as observations. (As in most applications of imperfect models to nature, we have already corrected for the mean state by using anomalies and correcting for overall amplitude error by rescaling using observed variance.) We use this rescaled model output to better understand forced PDO impacts, for instance, precipitation in the western United States. Label this impact variable *X;* it is the sum of a component X_{fPDO} that is a response to the forced PDO and an unforced component X_{res}. We find X_{fPDO} by linearly regressing *X* on the PDO index. Fig. S10 shows the result for precipitation over the U.S. X_{res} is then the residual $X - X_{fPDO}$. We separate this resultant field, X_{res}, into low-frequency $X_{LP}$and high-frequency components X_{HP}, by low-pass filtering the timeseries at each grid point. We then rescale both the forced component related to the PDO and the remaining low-frequency component so that the signal to noise in the model matches that estimated for the observations; i.e.

$$X' = \sqrt{\frac{R_j^2}{R_i^2}} * X_{fPDO} + \sqrt{\frac{1-R_j^2}{1-R_i^2}} * X_{LP} + X_{HP}$$

Note that the higher frequency variance (residual after low-pass filtering) remains at its original amplitude, and that the total LP variance is unchanged. The assumption that total variance remains constant affects the width of the resultant distributions, but not our ensemble mean results. We retain the model generated high-frequency variance simply to ensure the strongest possible tests of our results.

There are multiple potential sources of uncertainty in our estimate of the signal-to-noise ratio used for this recalibration. One testable source of uncertainty is the possibility that internal variability in observations aligns with the ensemble mean to artificially inflate our estimate of the observed signal-to-noise ratio. For our estimate of the signal-to-noise ratio in observations (R^2/1-R^2, 0.53/(1-0.53) = 1.13) to be so wrong as to be the same as in models (0.07/(1-0.07) = 0.08), the correlation between the ensemble mean and internal variability must exceed 0.62. This occurs in 1 out of our 572 ensemble members. This potentially thorny ensemble member simulates a 3.48% per 30 yrs increase in precipitation between 1983 - 2012 (relative to a 13.3% decrease in precipitation in observations). So, even if we accept the small chance that internal variability has confounded our understanding of the forced PDO - in this one extreme example present in the large ensemble, it does not explain the observed drought nor detract from our argument that the drought will continue to be forced moving forward.

Data and materials availability

All climate model output is publicly available via the Earth System Grid Federation's website, accessible at https://esgf.llnl.gov/. NOAA Extended Reconstructed SST V5 (ERSSTv5), NOAA/CIRES/DOE 20th Century Reanalysis (V3), and Global Precipitation Climatology Project (GPCP) Monthly Analysis Product data provided by the NOAA PSL, Boulder, Colorado, USA, from their website at https://psl.noaa.gov. Hadley Centre Sea Ice and Sea Surface Temperature (HadISST) data provided by the Met Office (UK) and available at their website at https://www.metoffice.gov.uk/hadobs/hadisst/.

References

1. Mantua, N. J., Hare, S. R., Zhang, Y., Wallace, J. M., & Francis, R. C., A Pacific Interdecadal Climate Oscillation with Impacts on Salmon Production. *Bulletin of the American Meteorological Society*, *78*(6), (1997). 1069–1080.
2. Zhang, Y., Wallace, J. M., & Battisti, D. S., ENSO-like Interdecadal Variability: 1900–93. *Journal of Climate*, *10*(5), (1997). 1004–1020.
3. Trenberth, K. E., & Fasullo, J. T., An apparent hiatus in global warming? *Earth's Future*, *1*(1), (2013). 19–32.
4. McCabe, G. J., Palecki, M. A., & Betancourt, J. L., Pacific and Atlantic Ocean influences on multidecadal drought frequency in the United States. *Proceedings of the National Academy of Sciences*, *101*(12), (2004). 4136–4141.
5. Newman, M., Alexander, M. A., Ault, T. R., Cobb, K. M., Deser, C., Lorenzo, E. D., Mantua, N. J., Miller, A. J., Minobe, S., Nakamura, H., Schneider, N., Vimont, D. J., Phillips, A. S., Scott, J. D., & Smith, C. A., The Pacific Decadal Oscillation, Revisited. *Journal of Climate*, *29*(12), (2016). 4399–4427.
6. Latif, M., & Barnett, T. P., Causes of Decadal Climate Variability over the North Pacific and North America. *Science*, *266*(5185), (1994). 634–637.
7. Eyring, V., N.P. Gillett, K.M. Achuta Rao, R. Barimalala, M. Barreiro Parrillo, N. Bellouin, C. Cassou, P.J. Durack, Y. Kosaka, S. McGregor, S. Min, O. Morgenstern, and Y. Sun, Human Influence on the Climate System. In Climate Change 2021: The Physical Science Basis. Contribution of Working Group I to the Sixth Assessment Report of the Intergovernmental Panel on Climate Change [Masson-Delmotte, V., P. Zhai, A. Pirani, S.L. Connors, C. Péan, S. Berger, N. Caud, Y. Chen, L. Goldfarb, M.I. Gomis, M. Huang, K. Leitzell, E. Lonnoy, J.B.R. Matthews, T.K. Maycock, T. Waterfield, O. Yelekçi, R. Yu, and B. Zhou (eds.)]. Cambridge University Press, Cambridge, United Kingdom and New York, NY, USA, (2021). 423–552.
8. Meehl, G. A., Hu, A., & Teng, H. (2016). Initialized decadal prediction for transition to positive phase of the Interdecadal Pacific Oscillation. *Nature Communications*, *7*(1), Article 1.
9. Dong, L., Zhou, T., & Chen, X., Changes of Pacific decadal variability in the twentieth century driven by internal variability, greenhouse gases, and aerosols. *Geophysical Research Letters*, *41*(23), (2014). 8570–8577.
10. Hua, W., Dai, A., & Qin, M., Contributions of Internal Variability and External Forcing to the Recent Pacific Decadal Variations. *Geophysical Research Letters*, *45*(14), (2018). 7084–7092.
11. Borchert, L. F., Koul, V., Menary, M. B., Befort, D. J., Swingedouw, D., Sgubin, G., & Mignot, J., Skillful decadal prediction of unforced southern European summer temperature variations. *Environmental Research Letters*, *16*(10), (2021). 104017.
12. Booth, B. B. B., Dunstone, N. J., Halloran, P. R., Andrews, T., & Bellouin, N., Aerosols implicated as a prime driver of twentieth-century North Atlantic climate variability. *Nature*, *484*(7393), (2012). 228.

13. Klavans, J. M., Cane, M. A., Clement, A. C., & Murphy, L. N., NAO predictability from external forcing in the late 20th century. *Npj Climate and Atmospheric Science*, *4*(1), (2021). 1–8.
14. Menary, M. B., Robson, J., Allan, R. P., Booth, B. B. B., Cassou, C., Gastineau, G., Gregory, J., Hodson, D., Jones, C., Mignot, J., Ringer, M., Sutton, R., Wilcox, L., & Zhang, R., Aerosol-Forced AMOC Changes in CMIP6 Historical Simulations. *Geophysical Research Letters*, *47*(14), (2020). e2020GL088166.
15. He, C., Clement, A. C., Kramer, S. M., Cane, M. A., Klavans, J. M., Fenske, T. M., & Murphy, L. N. (2023). Tropical Atlantic multidecadal variability is dominated by external forcing. *Nature*, *622*(7983), Article 7983.
16. Zhang, R., Sutton, R., Danabasoglu, G., Kwon, Y.-O., Marsh, R., Yeager, S. G., Amrhein, D. E., & Little, C. M. A Review of the Role of the Atlantic Meridional Overturning Circulation in Atlantic Multidecadal Variability and Associated Climate Impacts. *Reviews of Geophysics*, *57*(2), (2019) 316–375.
17. Wang, T., Otterå, O. H., Gao, Y., & Wang, H., The response of the North Pacific Decadal Variability to strong tropical volcanic eruptions. *Climate Dynamics*, *39*, (2012). 2917–2936.
18. Yeh, S.-W., Kim, W.-M., Kim, Y. H., Moon, B.-K., Park, R. J., & Song, C.-K., Changes in the variability of the North Pacific sea surface temperature caused by direct sulfate aerosol forcing in China in a coupled general circulation model. *Journal of Geophysical Research: Atmospheres*, *118*(3), (2013). 1261–1270.
19. Boo, K.-O., Booth, B. B. B., Byun, Y.-H., Lee, J., Cho, C., Shim, S., & Kim, K.-T., Influence of aerosols in multidecadal SST variability simulations over the North Pacific. *Journal of Geophysical Research: Atmospheres*, *120*(2), (2015). 517–531.
20. Diao, C., Xu, Y., & Xie, S.-P., Anthropogenic aerosol effects on tropospheric circulation and sea surface temperature (1980-2020): Separating the role of zonally asymmetric forcings. *Atmospheric Chemistry and Physics*, *21*(24), (2021). 18499–18518.
21. Allen, R. J., Norris, J. R., & Kovilakam, M., Influence of anthropogenic aerosols and the Pacific Decadal Oscillation on tropical belt width. *Nature Geoscience*, *7*(4), (2014). 270–274.
22. Smith, D. M., Booth, B. B. B., Dunstone, N. J., Eade, R., Hermanson, L., Jones, G. S., Scaife, A. A., Sheen, K. L., & Thompson, V., Role of volcanic and anthropogenic aerosols in the recent global surface warming slowdown. *Nature Climate Change*, *6*(10), (2016). 936–940.
23. Dittus, A. J., Hawkins, E., Robson, J., Smith, D. M., & Wilcox, L. J., Drivers of Recent North Pacific Decadal Variability: The Role of Aerosol Forcing. *Earths Future*, *9*(12), (2021). e2021EF002249.
24. Liguori, G., McGregor, S., Arblaster, J. M., Singh, M. S., & Meehl, G. A. (2020). A joint role for forced and internally-driven variability in the decadal modulation of global warming. *Nature Communications*, *11*(1), 3827.

25. Henley, B. J., Meehl, G., Power, S. B., Folland, C. K., King, A. D., Brown, J. N., Karoly, D. J., Delage, F., Gallant, A. J. E., Freund, M., & Neukom, R. (2017). Spatial and temporal agreement in climate model simulations of the Interdecadal Pacific Oscillation. *Environmental Research Letters*, *12*(4), 044011.
26. Mann, M. E., Steinman, B. A., & Miller, S. K. (2020). Absence of internal multidecadal and interdecadal oscillations in climate model simulations. *Nature Communications*, *11*(1), 1–9.
27. Zhao, Y., Newman, M., Capotondi, A., Lorenzo, E. D., & Sun, D. (2021). Removing the Effects of Tropical Dynamics from North Pacific Climate Variability. *Journal of Climate*, *34*(23), 9249–9265.
28. Heede, U. K., & Fedorov, A. V. (2023). Colder Eastern Equatorial Pacific and Stronger Walker Circulation in the Early 21st Century: Separating the Forced Response to Global Warming From Natural Variability. *Geophysical Research Letters*, *50*(3), e2022GL101020.
29. Solomon, A., & Newman, M. (2012). Reconciling disparate twentieth-century Indo-Pacific ocean temperature trends in the instrumental record. *Nature Climate Change*, *2*(9), 691–699.
30. Bonfils, C., & Santer, B. D., Investigating the possibility of a human component in various pacific decadal oscillation indices. *Climate Dynamics*, *37*(7), (2011). 1457–1468.
31. Ebisuzaki, W. (1997). A Method to Estimate the Statistical Significance of a Correlation When the Data Are Serially Correlated. *Journal of Climate*, *10* 2147–2153.
32.
33. Smith, D. M., Scaife, A. A., Eade, R., Athanasiadis, P., Bellucci, A., Bethke, I., Bilbao, R., Borchert, L. F., Caron, L.-P., Counillon, F., Danabasoglu, G., Delworth, T., Doblas-Reyes, F. J., Dunstone, N. J., Estella-Perez, V., Flavoni, S., Hermanson, L., Keenlyside, N., Kharin, V., … Zhang, L., North Atlantic climate far more predictable than models imply. *Nature*, *583*(7818), (2020). 796–800.
34. Scaife, A. A., Arribas, A., Blockley, E., Brookshaw, A., Clark, R. T., Dunstone, N., Eade, R., Fereday, D., Folland, C. K., Gordon, M., Hermanson, L., Knight, J. R., Lea, D. J., MacLachlan, C., Maidens, A., Martin, M., Peterson, A. K., Smith, D., Vellinga, M., … Williams, A., Skillful long-range prediction of European and North American winters. *Geophysical Research Letters*, *41*(7), (2014). 2514–2519.
35. Scaife, A. A., & Smith, D., A signal-to-noise paradox in climate science. *Npj Climate and Atmospheric Science*, *1*(1), (2018). 1–8.
36. Eade, R., Smith, D., Scaife, A., Wallace, E., Dunstone, N., Hermanson, L., & Robinson, N. (2014). Do seasonal-to-decadal climate predictions underestimate the predictability of the real world? *Geophysical Research Letters*, *41*(15), 5620–5628.
37. Waite, A. J., Klavans, J. M., Clement, A. C., Murphy, L. N., Liebetrau, V., Eisenhauer, A., Weger, R. J., & Swart, P. K. (2020). Observational and Model Evidence for an Important Role for Volcanic Forcing Driving Atlantic Multidecadal Variability Over the Last 600 Years. *Geophysical Research Letters*, *47*(23), e2020GL089428.

38. Deser, C., Phillips, A. S., Simpson, I. R., Rosenbloom, N., Coleman, D., Lehner, F., Pendergrass, A. G., DiNezio, P., & Stevenson, S., Isolating the Evolving Contributions of Anthropogenic Aerosols and Greenhouse Gases: A New CESM1 Large Ensemble Community Resource. *Journal of Climate*, *33*(18), (2020). 7835–7858.
39. Hoesly, R. M., Smith, S. J., Feng, L., Klimont, Z., Janssens-Maenhout, G., Pitkanen, T., Seibert, J. J., Vu, L., Andres, R. J., Bolt, R. M., Bond, T. C., Dawidowski, L., Kholod, N., Kurokawa, J., Li, M., Liu, L., Lu, Z., Moura, M. C. P., O'Rourke, P. R., & Zhang, Q., Historical (1750–2014) anthropogenic emissions of reactive gases and aerosols from the Community Emissions Data System (CEDS). *Geoscientific Model Development*, *11*(1), (2018). 369–408.
40. Frankignoul, C., Sennéchael, N., Kwon, Y.-O., & Alexander, M. A., Influence of the Meridional Shifts of the Kuroshio and the Oyashio Extensions on the Atmospheric Circulation. *Journal of Climate*, *24*(3), (2011). 762–777.
41. Anderson, B. T., Empirical Evidence Linking the Pacific Decadal Precession to Kuroshio Extension Variability. *Journal of Geophysical Research: Atmospheres*, *124*(23), (2019). 12845–12863.
42. Di Lorenzo, E., Xu, T., Zhao, Y., Newman, M., Capotondi, A., Stevenson, S., Amaya, D. J., Anderson, B. T., Ding, R., Furtado, J. C., Joh, Y., Liguori, G., Lou, J., Miller, A. J., Navarra, G., Schneider, N., Vimont, D. J., Wu, S., & Zhang, H., Modes and Mechanisms of Pacific Decadal-Scale Variability. *Annual Review of Marine Science*, *15*(1), (2023).
43. Fenske, T., & Clement, A. (2022). No Internal Connections Detected Between Low Frequency Climate Modes in North Atlantic and North Pacific Basins. *Geophysical Research Letters*, *49*(5), e2022GL097957.
44. Broccoli, A. J., Lau, N. C., & Nath, M. J. (1998). The cold ocean-warm land pattern: Model simulation and relevance to climate change detection. *Journal of Climate*, *11*(11), 2743–2763.
45. Laguë, M. M., Quetin, G. R., & Boos, W. R. (2022). Downwind control of oceanic air by land: The land wake and its sensitivity to CO2. *Environmental Research Letters*, *17*(10), 104045.
46. Kwon, Y.-O., & Deser, C., North Pacific Decadal Variability in the Community Climate System Model Version 2. *Journal of Climate*, *20*(11), (2007). 2416–2433.
47. Smirnov, D., Newman, M., Alexander, M. A., Kwon, Y.-O., & Frankignoul, C., Investigating the Local Atmospheric Response to a Realistic Shift in the Oyashio Sea Surface Temperature Front. *Journal of Climate*, *28*(3), (2015). 1126–1147.
48. Kosaka, Y., & Xie, S.-P., Recent global-warming hiatus tied to equatorial Pacific surface cooling. *Nature*, *501*(7467), (2013). 7467.
49. Seager, R., Cane, M., Henderson, N., Lee, D.-E., Abernathey, R., & Zhang, H., Strengthening tropical Pacific zonal sea surface temperature gradient consistent with rising greenhouse gases. *Nature Climate Change*, *9*(7), (2019). 517–522.
50. Maher, N., Wills, R. C. J., DiNezio, P., Klavans, J., Milinski, S., Sanchez, S. C., Stevenson, S., Stuecker, M. F., & Wu, X., The future of the El Niño-Southern

Oscillation: Using large ensembles to illuminate time-varying responses and inter-model differences. *Earth System Dynamics Discussions*, (2022). 1–28.

51. Clement, A. C., Seager, R., Cane, M. A., & Zebiak, S. E., An Ocean Dynamical Thermostat. *Journal of Climate*, *9*(9), (1996). 2190–2196.
52. Cane, M. A., Clement, A. C., Kaplan, A., Kushnir, Y., Pozdnyakov, D., Seager, R., Zebiak, S. E., & Murtugudde, R., Twentieth-Century Sea Surface Temperature Trends. *Science*, *275*(5302), (1997). 957–960.
53. Lehner, F., Deser, C., Simpson, I. R., & Terray, L., Attributing the U.S. Southwest's Recent Shift Into Drier Conditions. *Geophysical Research Letters*, *45*(12), (2018). 6251–6261.
54. Mankin J.S., Simpson I., Hoell A., Fu R., Lisonbee J., Sheffield A., Barrie D., NOAA Drought Task Force Report on the 2020–2021 Southwestern U.S. Drought. NOAA Drought Task Force, MAPP, and NIDIS (2021).
55. Seager, R., & Ting, M. Decadal Drought Variability Over North America: Mechanisms and Predictability. *Current Climate Change Reports*, *3*(2), (2017), 141–149.
56. McCabe, G. J., & Dettinger, M. D. (1999). Decadal variations in the strength of ENSO teleconnections with precipitation in the western United States. *International Journal of Climatology*, *19*(13), 1399–1410.
57. Yeager, S. G., Danabasoglu, G., Rosenbloom, N. A., Strand, W., Bates, S. C., Meehl, G. A., Karspeck, A. R., Lindsay, K., Long, M. C., Teng, H., & Lovenduski, N. S. Predicting Near-Term Changes in the Earth System: A Large Ensemble of Initialized Decadal Prediction Simulations Using the Community Earth System Model. *Bulletin of the American Meteorological Society*, *99*(9), (2018), 1867–1886.
58. Scaife, A. A., Camp, J., Comer, R., Davis, P., Dunstone, N., Gordon, M., MacLachlan, C., Martin, N., Nie, Y., Ren, H.-L., Roberts, M., Robinson, W., Smith, D., & Vidale, P. L., Does increased atmospheric resolution improve seasonal climate predictions? *Atmospheric Science Letters*, *20*(8), (2019). e922.
59. Hardiman, S. C., Dunstone, N. J., Scaife, A. A., Smith, D. M., Comer, R., Nie, Y., & Ren, H.-L., Missing eddy feedback may explain weak signal-to-noise ratios in climate predictions. *Npj Climate and Atmospheric Science*, *5*(1), (2022). 1–8.
60. Siqueira, L., & Kirtman, B. P., Atlantic near-term climate variability and the role of a resolved Gulf Stream. *Geophysical Research Letters*, *43*(8), (2016). 3964–3972.
61. Zhang, W., Kirtman, B., Siqueira, L., Clement, A., & Xia, J., Understanding the signal-to-noise paradox in decadal climate predictability from CMIP5 and an eddying global coupled model. *Climate Dynamics*, *56*(9), (2021). 2895–2913.
62. Murphy, L. N., Klavans, J. M., Clement, A. C., & Cane, M. A. (2021). Investigating the Roles of External Forcing and Ocean Circulation on the Atlantic Multidecadal SST Variability in a Large Ensemble Climate Model Hierarchy. *Journal of Climate*, *1*(aop), 1–51.
63. Kay, J. E., Deser, C., Phillips, A., Mai, A., Hannay, C., Strand, G., Arblaster, J. M., Bates, S. C., Danabasoglu, G., Edwards, J., Holland, M., Kushner, P., Lamarque, J.-F., Lawrence, D., Lindsay, K., Middleton, A., Munoz, E., Neale, R., Oleson, K., …

Vertenstein, M. The Community Earth System Model (CESM) Large Ensemble Project: A Community Resource for Studying Climate Change in the Presence of Internal Climate Variability. *Bulletin of the American Meteorological Society*, *96*(8), (2015). 1333–1349.

64. Gillett, N. P., Shiogama, H., Funke, B., Hegerl, G., Knutti, R., Matthes, K., Santer, B. D., Stone, D., & Tebaldi, C., The Detection and Attribution Model Intercomparison Project (DAMIP v1.0) contribution to CMIP6. *Geoscientific Model Development*, *9*(10), (2016). 3685–3697.
65. Huang, B., Thorne, P. W., Banzon, V. F., Boyer, T., Chepurin, G., Lawrimore, J. H., Menne, M. J., Smith, T. M., Vose, R. S., & Zhang, H.-M., Extended Reconstructed Sea Surface Temperature, Version 5 (ERSSTv5): Upgrades, Validations, and Intercomparisons. *Journal of Climate*, *30*(20), (2017). 8179–8205.
66. Rayner, N. A., Parker, D. E., Horton, E. B., Folland, C. K., Alexander, L. V., Rowell, D. P., Kent, E. C., & Kaplan, A., Global analyses of sea surface temperature, sea ice, and night marine air temperature since the late nineteenth century. *Journal of Geophysical Research: Atmospheres*, *108*(D14), (2003).
67. Hirahara, S., Ishii, M., & Fukuda, Y., Centennial-Scale Sea Surface Temperature Analysis and Its Uncertainty. *Journal of Climate*, *27*(1), (2014). 57–75.
68. Schneider, U., Becker, A., Finger, P., Meyer-Christoffer, A., Ziese, M., & Rudolf, B., GPCC's new land surface precipitation climatology based on quality-controlled in situ data and its role in quantifying the global water cycle. *Theoretical and Applied Climatology*, *115*(1), (2014). 15–40.
69. Mantua, N. J., & Hare, S. R., The Pacific Decadal Oscillation. *Journal of Oceanography*, *58*(1), (2002). 35–44.
70. Jeffrey, S., Rotstayn, L., Collier, M., Dravitzki, S., Hamalainen, C., Moeseneder, C., Wong, K., & Syktus, J., Australia's CMIP5 submission using the CSIRO Mk3. 6 model. *Aust. Meteor. Oceanogr. J*, *63*, (2013). 1–13.
71. Rodgers, K. B., Lin, J., & Frölicher, T. L., Emergence of multiple ocean ecosystem drivers in a large ensemble suite with an Earth system model. *Biogeosciences*, *12*(11), (2015). 3301–3320.
72. Kirchmeier-Young, M. C., Zwiers, F. W., & Gillett, N. P., Attribution of extreme events in Arctic sea ice extent. *Journal of Climate*, *30*(2), (2017). 553–571.
73. Sun, L., Alexander, M., & Deser, C., Evolution of the global coupled climate response to Arctic sea ice loss during 1990–2090 and its contribution to climate change. *Journal of Climate*, *31*(19), (2018). 7823–7843.
74. Maher, N., Milinski, S., Suarez-Gutierrez, L., Botzet, M., Dobrynin, M., Kornblueh, L., Kröger, J., Takano, Y., Ghosh, R., Hedemann, C., Li, C., Li, H., Manzini, E., Notz, D., Putrasahan, D., Boysen, L., Claussen, M., Ilyina, T., Olonscheck, D., Marotzke, J., The Max Planck Institute Grand Ensemble: Enabling the Exploration of Climate System Variability. *Journal of Advances in Modeling Earth Systems*, *11*(7), (2019). 2050–2069.
75. Rodgers, K. B., Lee, S.-S., Rosenbloom, N., Timmermann, A., Danabasoglu, G., Deser, C., Edwards, J., Kim, J.-E., Simpson, I. R., Stein, K., Stuecker, M. F., Yamaguchi, R.,

Bódai, T., Chung, E.-S., Huang, L., Kim, W. M., Lamarque, J.-F., Lombardozzi, D. L., Wieder, W. R., & Yeager, S. G., Ubiquity of human-induced changes in climate variability. *Earth System Dynamics*, *12*(4), (2021).1393–1411.

76. Delworth, T. L., Cooke, W. F., Adcroft, A., Bushuk, M., Chen, J.-H., Dunne, K. A., Ginoux, P., Gudgel, R., Hallberg, R. W., Harris, L., Harrison, M. J., Johnson, N., Kapnick, S. B., Lin, S.-J., Lu, F., Malyshev, S., Milly, P. C., Murakami, H., Naik, V., … Zhao, M., SPEAR: The Next Generation GFDL Modeling System for Seasonal to Multidecadal Prediction and Projection. *Journal of Advances in Modeling Earth Systems*, *12*(3), (2020). e2019MS001895.
77. Bonnet, R., Boucher, O., Deshayes, J., Gastineau, G., Hourdin, F., Mignot, J., Servonnat, J., & Swingedouw, D., Presentation and Evaluation of the IPSL-CM6A-LR Ensemble of Extended Historical Simulations. *Journal of Advances in Modeling Earth Systems*, *13*(9), (2021). e2021MS002565.
78. Tatebe, H., Ogura, T., Nitta, T., Komuro, Y., Ogochi, K., Takemura, T., Sudo, K., Sekiguchi, M., Abe, M., Saito, F., Chikira, M., Watanabe, S., Mori, M., Hirota, N., Kawatani, Y., Mochizuki, T., Yoshimura, K., Takata, K., O'ishi, R., Kimoto, M., Description and basic evaluation of simulated mean state, internal variability, and climate sensitivity in MIROC6. *Geoscientific Model Development*, *12*(7), (2019). 2727–2765.
79. Fyfe, J. C., Kharin, V. V., Santer, B. D., Cole, J. N. S., & Gillett, N. P., Significant impact of forcing uncertainty in a large ensemble of climate model simulations. *Proceedings of the National Academy of Sciences*, *118*(23), (2021). e2016549118.
80. Ziehn, T., Chamberlain, M. A., Law, R. M., Lenton, A., Bodman, R. W., Dix, M., Stevens, L., Wang, Y.-P., Srbinovsky, J., Ziehn, T., Chamberlain, M. A., Law, R. M., Lenton, A., Bodman, R. W., Dix, M., Stevens, L., Wang, Y.-P., & Srbinovsky, J., The Australian Earth System Model: ACCESS-ESM1.5. *Journal of Southern Hemisphere Earth Systems Science*, *70*(1), (2020). 193–214.

Acknowledgments

We are grateful for helpful comments from John Fasullo, Jennifer Kay, Isla Simpson.

Funding

National Science Foundation grant AGS-2002528 (JK, PD, TS)

NOAA Climate Program Office grant NA20OAR4310400 and National Science Foundation grant AGS-2241752 (AC)

The National Center for Atmospheric Research is sponsored by the National Science Foundation.

Author contributions:

Conceptualization: JK, PD

Methodology: JK, PD, MC

Investigation: JK

Visualization: JK

Funding acquisition: PD, TS

Writing – original draft: JK

Writing – review & editing: JK, PD, AC, CD, TS, MC

Competing interests

Authors declare that they have no competing interests.

Additional Information

Supplementary Information is available for this paper. Correspondence and requests for materials should be addressed to Jeremy Klavans (jeremy.klavans@colorado.edu). Reprints and permissions information is available at www.nature.com/reprints.

Supplementary Materials

Figs. S1 to S11

Tables S1 to S7

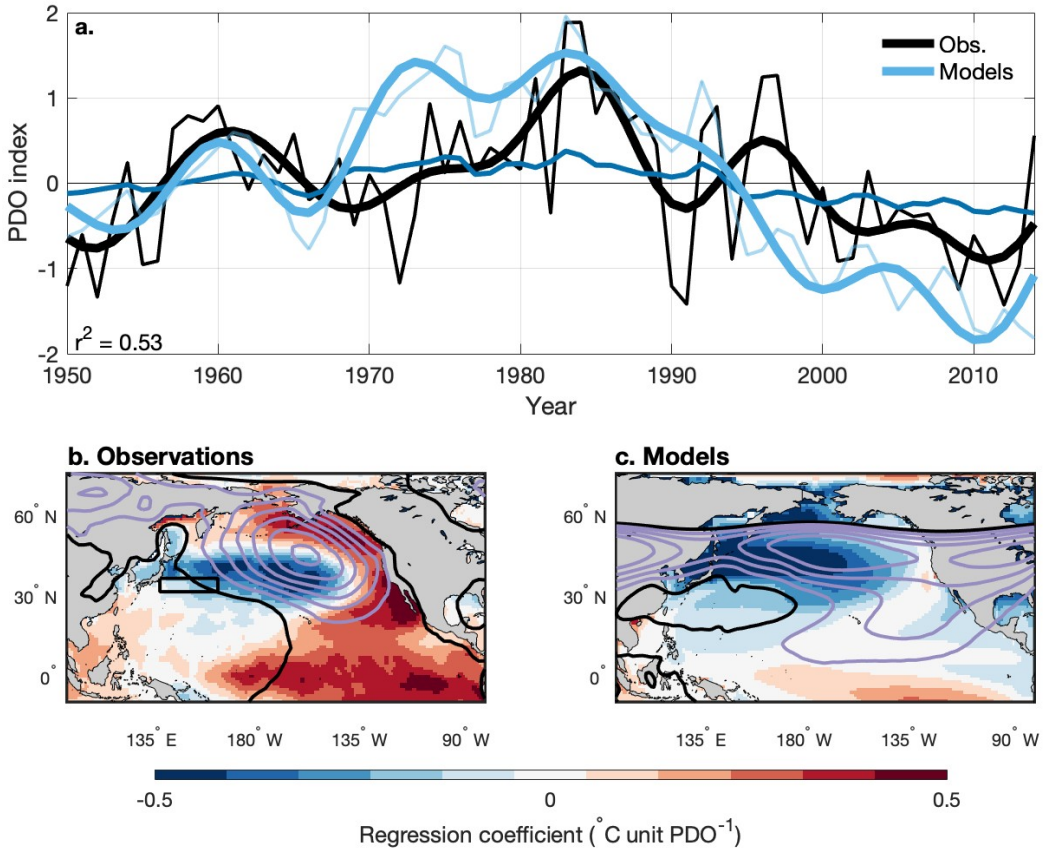

Fig. 1. External forcing explains the timing and pattern of the PDO. (a) The observed PDO index with ENSO linearly removed (black) compared with the ensemble mean PDO index from the all-forcings simulations (dark blue) and the normalized ensemble mean PDO index from the all-forcings simulations (light blue). We normalize the forced PDO index by setting the standard deviation to one to maintain consistency with the traditional definition of the PDO index (*1*) and to illustrate the timing of the shifts in both indices; the amplitudes of each timeseries are listed in Table S5 and discussed in-text. The R^2 value in the bottom left is the square of the correlation between the observed (ENSO removed) and ensemble mean PDO indices. (b) Regression of observed SST (colors; °C per unit of the PDO index) and sea-level pressure (contours; hPa per unit of the PDO index) on the observed PDO index. The KOE region is outlined in the solid black rectangle. (c) Regression of ensemble mean SST (colors) and sea-level pressure (contours) on the normalized, ensemble mean PDO index from the all-forcings simulations (see text for details). In panels b) and c), SLP regressions are contoured every 0.5 hPa; negative values are in purple and the zero contour is in black (there are no positive values).

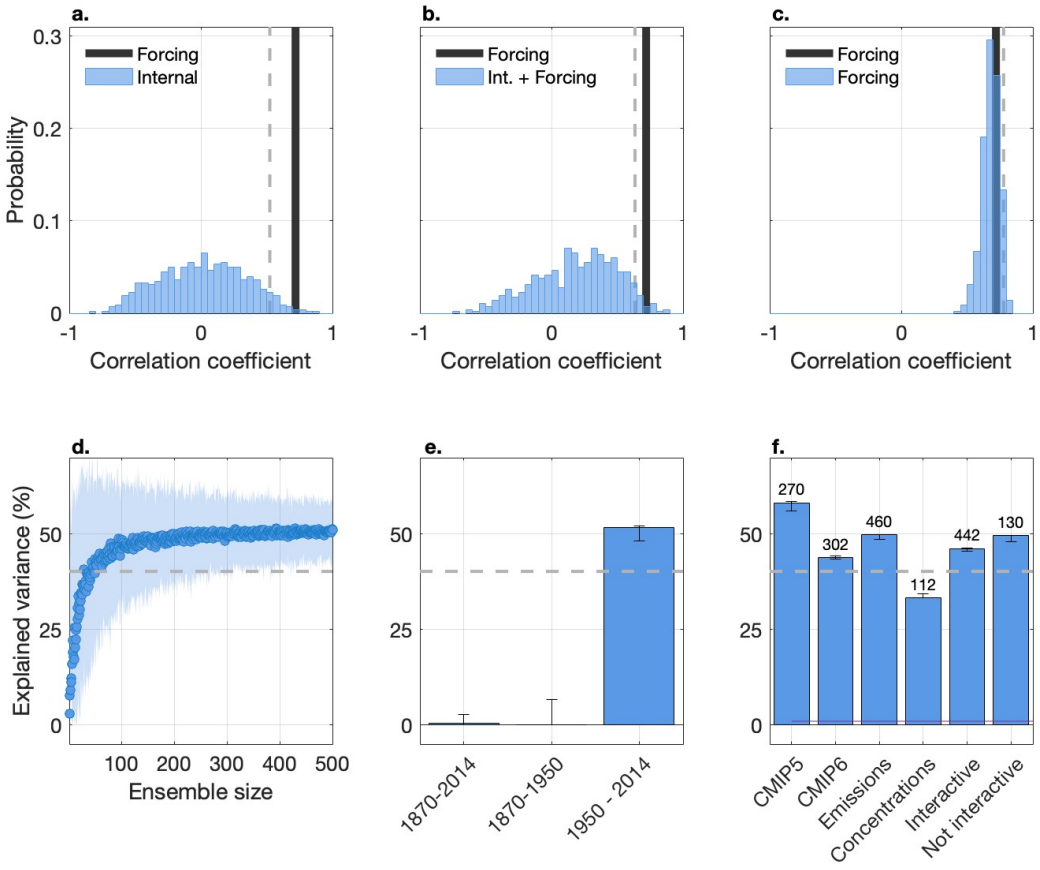

Fig. 2. The robustness of the role of forcing in the PDO. (a) Comparison of the correlation coefficient between the internally-generated PDO indices in individual ensemble members and observations (blue histogram) with the correlation coefficient of the ensemble mean and observation (black vertical line). The empirical 90% confidence level (two-tailed) for the distribution of correlations is displayed with a light gray vertical line. (b) As in (a), but for the PDO index from each individual ensemble member which includes internally generated and externally forced variability. (c) as in (a) and (b), but for bootstrapped 100-member ensemble means that illustrate different estimates of the externally forced response. (d) The level of PDO variance explained by external forcing, as a function of ensemble size. For each ensemble size, we randomly select members from the full ensemble, average, and correlate with observations to calculate the mean explained variance (dot) and the 95% confidence interval (cloud). We also test the null hypothesis that there is no correlation at the 90% confidence level (gray dashed line). One can produce a conservative estimate of the ensemble size required to isolate the forced PDO by intersecting the bottom of the confidence interval at 500 members with the mean variance explained. (e) The contribution of external forcing to the PDO as a function of time in the full ensemble. Error bars are calculated via bootstrap (Methods). (f) Level of explained variance in the ensemble subdivided by key traits (see Table S1).

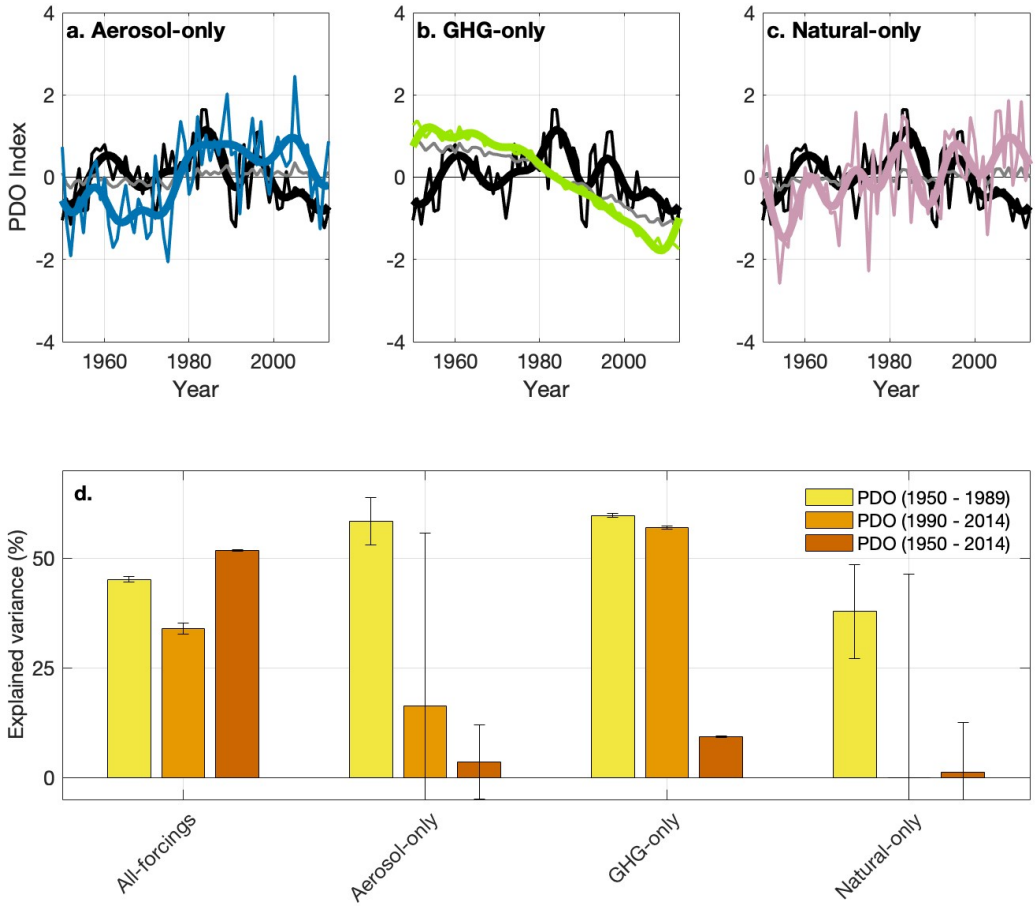

Fig. 3. Forcing from anthropogenic aerosols and greenhouse gases explain the timing of the PDO index. As in (Fig. 1a) but for the forced PDO index from the aerosol-only simulations (a), greenhouse gas-only simulations (b), and the natural forcing-only simulations (c). The original amplitude PDO index from each single-forcing ensemble is shown in the thin gray line. (d) The amount of observed PDO variance explained by the ensemble mean of each of the four suites of simulations for 1950 – 1989, 1990 – 2014, and 1950 – 2014 (bars) and their 90% confidence interval calculated via bootstrap as in Fig. 2d. This statistical test accounts for uncertainty in the forced response; a statistical test that compares these correlations to that which would have been produced from internal variability is presented in Table S6. Note that the correlation between the forced PDO in the GHG-only ensemble and observations between 1950 – 1989 is negative.

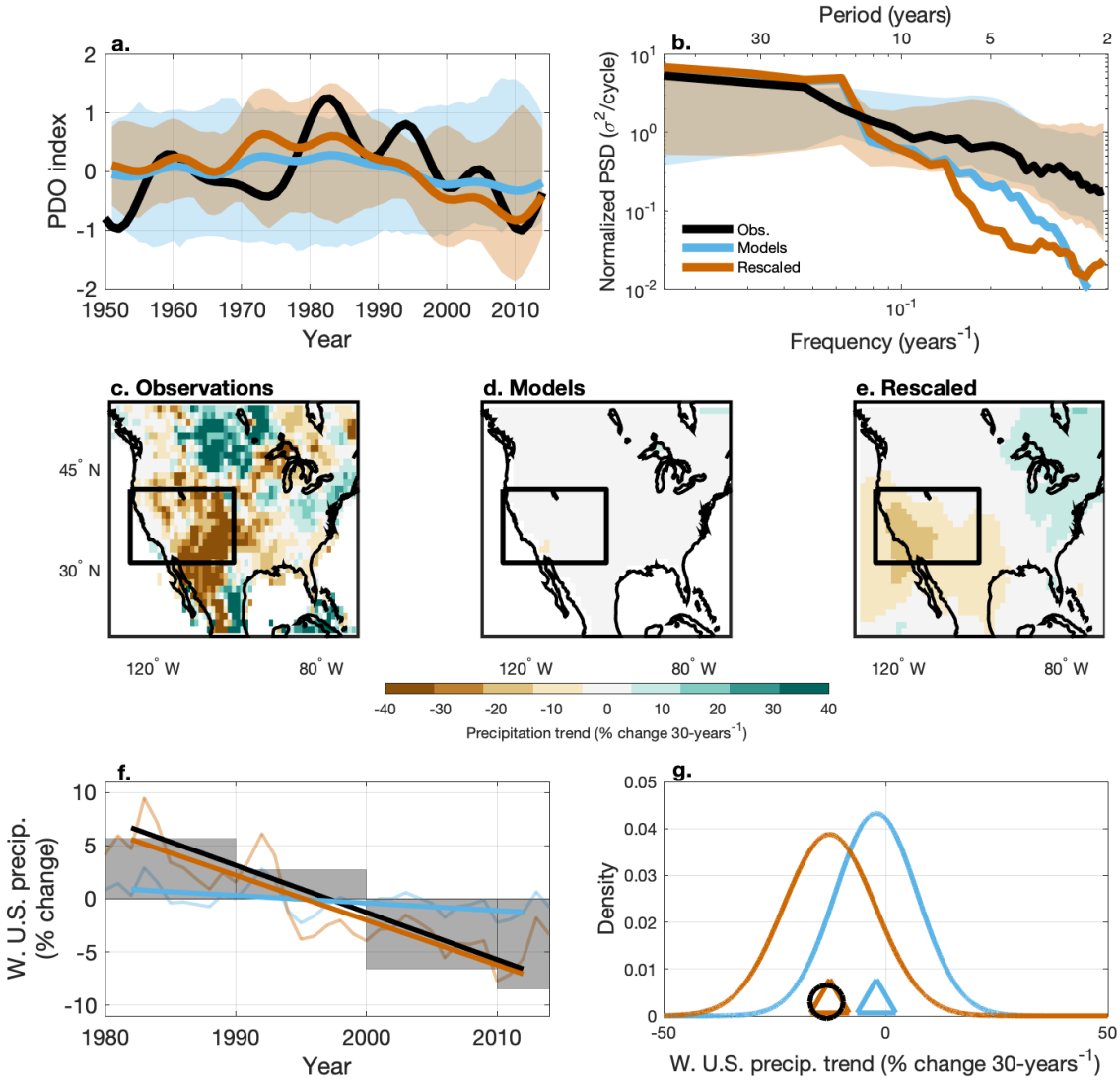

Fig. 4. Long-term meteorological drought in the western U.S. is attributable to human emissions of aerosols and greenhouse gases via their influence on the PDO. (a) The PDO indices from observations (black), the all-forcings large ensemble and ensemble mean (blue cloud and line), and the corrected ensemble and its ensemble mean (orange cloud and line). (b) Spectra of the PDO indices from observations (black), the all-forcings ensemble and ensemble mean (blue cloud and line), and corrected ensemble and ensemble mean (orange cloud and line). (c – d) Maps of water year (Oct. – Sep.) precipitation trends between 1983 – 2012 in observations, where the ENSO-related pattern of precipitation has been removed (c), the all-forcings ensemble (d), and the corrected ensemble (e). (f) Decadal mean precipitation changes in the western U.S. (31° - 42°N, 125° – 100°W) from observations, where ENSO has been removed (gray bars) and the timeseries of the forced precipitation changes from the all-forcings large ensemble (light blue) and the corrected ensemble (light orange). The best-fit linear trend is plotted for observations (black), the all-forcings ensemble mean (blue), and the corrected ensemble mean (orange). (g) Precipitation trends in the western US from observations (black circle), the all-forcings ensemble mean (blue triangle), the corrected ensemble mean (orange

triangle), and PDFs of the trends from individual all-forcing ensemble simulations (blue curve) and the corrected ensemble (orange curve).

840